Open Source MATLAB Implementation of Consistent Discretisations on Complex Grids

Knut–Andreas Lie Stein Krogstad Ingeborg S. Ligaarden
Jostein R. Natvig Halvor Møll Nilsen Bård Skaflestad

Received: date / Accepted: date

Abstract

Accurate geological modelling of features such as faults, fractures or erosion requires grids that are flexible with respect to geometry. Such grids generally contain polyhedral cells and complex grid cell connectivities. The grid representation for polyhedral grids in turn affects the efficient implementation of numerical methods for subsurface flow simulations.

Methods based on two-point flux approximations are known not to converge on grids that are not K orthogonal. In recent years, there has been significant research into mixed, multipoint, and mimetic discretisation methods that are all consistent and convergent. Furthermore, so-called multiscale methods have lately received a lot of attention.

In this paper we consider a MATLAB® implementation of consistent and convergent methods on unstructured, polyhedral grids. The main emphasis is put on flexibility and efficiency with respect to different grid formats, and in particular hierarchical grids used in multiscale methods. Moreover, we discuss how generic implementations of various popular methods for pressure and transport ease the study and development of advanced techniques such as multiscale methods and applications such as optimal control or well placement.

1 Introduction

Reliable computer modelling of subsurface flow is much needed to overcome important challenges such as sustainable use and management of the earth's groundwater systems, geological storage of CO_2 to mitigate the anthropological increases in the carbon content of the atmosphere, and optimal utilisation of hydrocarbon reservoirs. Indeed, the need for tools that help us understand flow processes in the subsurface is probably greater than ever, and increasing. More than fifty years of prior research in this area has led to some degree of agreement in terms of how subsurface flow processes can be modelled adequately with numerical simulation technology.

To describe the subsurface flow processes mathematically, two types of models are needed. First, one needs a mathematical model that describes how fluids flow in a porous medium. These models are typically given as a set of partial differential equations describing the mass-conservation of fluid phases, accompanied by a suitable set of constitutive relations. Second, one needs a geological model that describes the given porous rock formation (the reservoir). The geological model is realised as a grid populated with petrophysical or hydrological properties that are used as input to the flow model, and together they make up the reservoir simulation model. The geological model must also describe the geometry of the reservoir rock and in particular model geological horizons and major faults. This requires grids that are flexible with respect to geometry (and topology). Stratigraphic grids have been popular for many years and are the current industry standard. These grids are formed by extruding areal grids defined along geological surfaces to form volumetric descriptions. However, more complex methods based on unstructured grids are gaining in popularity as a means to modelling complex fault systems, horizontal and multilateral wells, etc. In either case, grids representing realistic reservoirs generally contain polyhedral cells and complex grid cell connectivities. The grid representation for polyhedral grids in turn affects the efficient implementation of numerical methods for subsurface flow simulations.

The industry-standard for discretising flow equations is the two-point flux-approximation method, which for a 2D Cartesian grid corresponds to a standard five-point scheme for the elliptic Poisson equation. Although widely used, this method is known not to converge on grids that are not K-orthogonal. In recent years, there has been significant research into mixed [7], multipoint [4], and mimetic [8] discretisation methods that are all consistent and convergent on rougher grids. Herein, we will focus on low-order, cell-centred methods that do not require specific reference elements and thus can be applied to grids with general polygonal and polyhedral cells.

Another major research challenge is the gap between simulation capabilities and the level of detail available in current geological models. Despite an astonishing increase in computer power, and intensive research on computation techniques, commercial reservoir simulators can seldom run simulations directly on highly resolved geological grid models that may contain from one to a hundred million cells. Instead, coarse-grid models with grid-blocks that are typically ten to a thousand times larger are built using some kind of upscaling of the geophysical parameters [15, 12]. How one should perform this upscaling is not trivial. In fact, upscaling has been, and probably still is, one of the most active research areas in the oil industry. Lately, however, so-called multiscale methods [16, 14, 17] have received a lot of attention. In these methods, coarsening and upscaling needed to reduce the number of degrees of freedom to a level that is sufficient to resolve flow physics and satisfy requirements on computational costs is done implicitly by the simulation method.

A major goal of the activities in our research group is to develop efficient simulation methodologies based on accurate and robust discretisation methods; in particular, we have focused on developing multiscale methods. To this end, we need a toolbox for rapid prototyping of new ideas that enables us to easily test the new implementations on a wide range of models, from small and highly idealised grid models to large models with industry-standard complexity. When developing new computational methodologies, flexibility and low development time is more important than high code efficiency, which will typically only be fully achieved after the experimental programming is completed and ideas have been thoroughly tested. For a number of years, we have therefore divided our code development in two parts: For prototyping and testing of new ideas, we have used MATLAB, whereas solvers aimed at high computational performance have been developed in a compiled language (i.e., using FORTRAN, C, or generic programming in C++).

This has resulted in a comprehensive set of routines and data structures for reading, representing, processing, and visualising unstructured grids, with particular emphasis on the corner-point format used within the petroleum industry and hierarchical grids used in multiscale methods. To enable other researchers to benefit from our efforts, these routines have been gathered in the MATLAB Reservoir Simulation Toolbox (MRST), which is released under the GNU General Public License (GPL). The first releases are geared towards single- and two-phase flow and contain a set of mimetic and multiscale flow solvers and a few simple transport solvers capable of handling general unstructured, polyhedral grids.

The main purpose of this paper is to present MRST and demonstrate its flexibility and efficiency with respect to different grid formats, and in particular hierarchical grids used in multiscale methods. Secondly, we present a class of mimetic methods that incorporates several well-known discretisation methods as special cases on simple grid while at the same time providing consistent discretistions on grids that are not K-orthogonal. Finally, we discuss how generic implementations of various popular methods for pressure and transport ease the study and development of advanced techniques such as multiscale methods, flow-based gridding, and applications such as optimal control or well placement.

2 The Matlab Reservoir Simulation Toolbox

The toolbox has the following functionality for rapid prototyping of solvers for flow and transport:

- grid structure, grid factory routines, input/processing of industry-standard formats, real-life and synthetic example grids
- petrophysical parameters and incompressible fluid models (our in-house development version also has support for compressible black-oil fluids), very simplified geostatistical routines
- routines for setting and manipulating boundary conditions, sources/sinks, and well models
- structure for reservoir state (pressure, fluxes, saturations, compositions, ...)

- visualisation routines for scalar cell and face data

Additionally, the toolbox contains several flow and transport solvers which may be readily combined using an operator splitting framework. In particular, we provide an implementation of the multiscale mixed finite-element method [3], working on unstructured, polyhedral grids.

The toolbox assumes that all physical quantities are given in a consistent system of units, preferably the strict SI system. However, to assist the user, MRST provides conversion to/from common units in reservoir description.

We will now go into more details about some of the components outlined above. The interested reader should also review the tutorials included in the current release.

2.1 Grids

A key requirement for MRST is that it should support a large variety of grid types. To avoid having a large number of different and potentially incompatible grid representations, all grids in MRST are assumed to consist of a set of non-overlapping polyhedral cells, where each cell can have a varying number of planar faces that match the faces of the cell's neighbours. Grids with non-matching faces, e.g., corner-point and other extruded grids, are therefore converted into matching grids by splitting non-matching faces into a set of matching (sub)faces. All grids are stored in a general format in which we explicitly represent cells, faces, and vertexes and the connections between cells and faces. Hence, we have sacrificed some of the efficiency attainable by exploiting special structures in a particular grid type for the sake of generality and flexibility.

The grid structure in MRST contains three fields—`cells`, `faces`, and `nodes`—that specify individual properties for each individual cell/face/vertex in the grid. The `nodes` structure is simple, it contains the number of nodes N_n and an $N_n \times d$ array of physical nodal coordinates in $\mathbb{R}^d$. The `cells` structure contains the number of cells N_c, an array `cells.faces` giving the global faces connected to a given cell, and an indirection map into `cells.faces` that gives the number of faces per cell. The `cells.faces` array has $n_f \times 2$ elements defined so that if `cells.faces(i,1)==j`, then global face `cells.faces(i,2)` is connected to global cell number j. To conserve memory, only the last column is stored, whereas the first column can be derived from a run-length encoding of the indirection map. The `cells` structure may optionally contain an array that maps internal cell indexes to external cell indexes, which is useful e.g., if the model contains inactive cells. Likewise, the `faces` structure contains the number of global faces, an array `faces.nodes` of vertexes connected to each face, an indirection map, and an array `neighbors` giving neighbouring information (face i is shared by global cells `neighbors(i,1)` and `neighbors(i,2)`). In addition, the grid may contain a label `type` which records the grid construction history. Finally, grids supporting an underlying logical Cartesian structure also include the field `cartDims`. The grid structure is illustrated in Figure 1 for a triangular grid with eight cells.

MRST contains several grid-factory routines for creating structured grids,

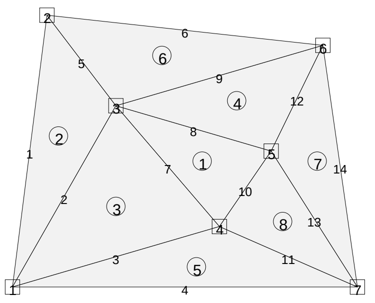

```
cells.faces =     faces.nodes =    faces.neighbors =
   1  10             1   1            0   2
   1   8             1   2            2   3
   1   7             2   1            3   5
   2   1             2   3            5   0
   2   2             3   1            6   2
   2   5             3   4            0   6
   3   3             4   1            1   3
   3   7             4   7            4   1
   3   2             5   2            6   4
   4   8             5   3            1   8
   4  12             6   2            8   5
   4   9             6   6            4   7
   5   3             7   3            7   8
   5   4             7   4            0   7
   5  11             8   3
   6   9             8   5
   6   6             9   3
   6   5             9   6
   7  13            10   4
   7  14            10   5
   :   :             :   :
```

Figure 1: Illustration of the `cell` and `faces` fields of the grid structure: cell numbers are marked by circles, node numbers by squares, and face numbers have no marker.

including regular Cartesian, rectilinear, and curvilinear grids, as well as unstructured grids, including Delaunay triangulations and Voronoi grids, and 3D grids created by extrusion of 2D shapes. Most important, however, is the support for the industry-standard corner-point grids given by the Eclipse input deck. In Figure 2 we show four examples of grids and the commands necessary to create and display them.

As we will see below, specific discretisation schemes may require other properties not supported by our basic grid class: cell volumes, cell centroids, face areas, face normals, and face centroids. Although these properties can be computed from the geometry (and topology) on the fly, it is often useful to precompute and include them explicitly in the grid structure `G`. This is done by calling the generic routine `G=computeGeometry(G)`.

2.2 Petrophysical Parameters

All flow and transport solvers in MRST assume that the rock parameters are represented as fields in a structure. Our naming convention is that this structure is called `rock`, but this is not a requirement. The fields for porosity and permeability, however, must be called `poro` and `perm`, respectively. The porosity field `rock.poro` is a vector with one value for each active cell in the corresponding grid model. The permeability field `rock.perm` can either contain a single column for an isotropic permeability, two or three columns for a diagonal permeability (in two and three spatial dimensions, respectively), or three or six columns for a symmetric, full tensor permeability (in two and three spatial dimensions, respectively). In the latter case, cell number i has the permeability tensor

$$\mathsf{K}_i = \begin{bmatrix} K_1(i) & K_2(i) \\ K_2(i) & K_3(i) \end{bmatrix}, \qquad \mathsf{K}_i = \begin{bmatrix} K_1(i) & K_2(i) & K_3(i) \\ K_2(i) & K_4(i) & K_5(i) \\ K_3(i) & K_5(i) & K_6(i) \end{bmatrix},$$

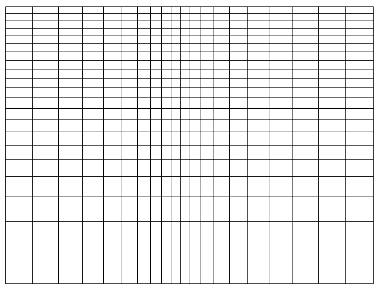

```
dx = 1-0.5*cos((-1:0.1:1)*pi);
x = -1.15+0.1*cumsum(dx);
G = tensorGrid(x, sqrt(0:0.05:1));
plotGrid(G);
```

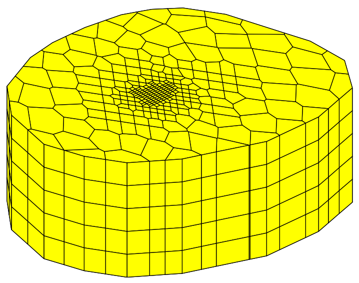

```
load seamount % Matlab standard dataset
g = pebi( tri2grid( delaunay(x,y),[x(:) y(:)]))
G = makeLayeredGrid(g, 5);
plotGrid(G), view(-40, 60),
```

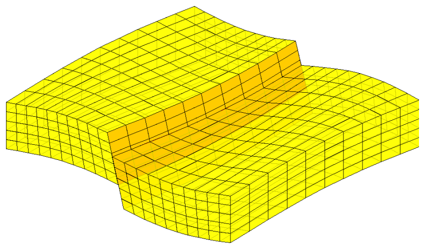

```
G = processGRDECL( ...
    simpleGrdecl([20, 10, 5], 0.12));
plotGrid(G,'FaceAlpha',0.8);
plotFaces(G,find( G.faces.tag >0), ...
   'FaceColor','red');
view(40,40), axis off
```

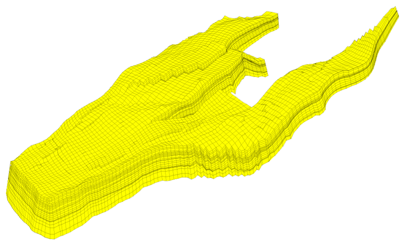

```
grdecl = readGRDECL('GSmodel.grdecl');
G = processGRDECL( grdecl );
G=G(1); % pick 1st of two disconnected parts
plotGrid(G,'EdgeAlpha',0.1);
view(0,70), axis tight off
```

Figure 2: Examples of grids and the MRST statements necessary to create them. The upper-left plot shows a standard tensor-product Cartesian grid. In the upper-right plot we start from an unstructured point set (the data file `seamount.mat` that is distributed with MATLAB), from which we create a 2D Voronoi grid that is extruded to a 3D model consisting of five layers. The lower-left plot shows an example of a corner-point grid with a single sloping fault and wavy top- and bottom surfaces. The lower-right plot shows a real reservoir from offshore Norway; the data file `GSmodel.grdecl` is unfortunately not yet available for public download.

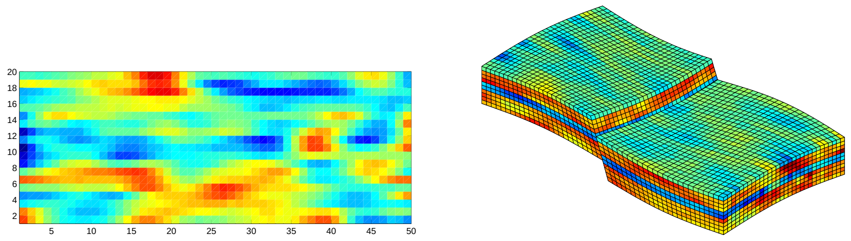

Figure 3: Two examples of MRST's simplified geostatistics. The left plot shows a 50×20 porosity field generated as a Gaussian field with a larger filter size in the x-direction than in the y-direction. The right plot shows a stratigraphic grid with a single fault and four geological layers, each with a log-normal permeability distribution.

where $K_j(i)$ is the entry in column j and row i of `rock.perm`. Full-tensor, non-symmetric permeabilities are currently not supported in MRST. In addition to porosity and permeability, MRST supports a field called `ntg` that represents the net-to-gross ratio and consists of either a scalar or a single column with one value per active cell.

Given the difficulty of measuring rock properties, it is common to use geostatistical methods to make realisations of porosity and permeability. MRST contains two very simplified methods for generating geostatistical realisations. As a simple approximation to a Gaussian field, we generate a field of independent, normally distributed variables and convolve it with a Gaussian kernel. This method is used in two different routines, `gaussianField` and `logNormLayers` that are illustrated in the following examples.

Example 1 (Random Petrophysical Variables) *First, we generate the porosity ϕ as a Gaussian field taking values in the interval $[0.2, 0.4]$. To get a crude approximation to the permeability-porosity relationship, we assume that our medium is made up of uniform spherical grains of diameter $d_p = 10\,\mu\mathrm{m}$, for which the specific surface area is $A_v = 6/d_p$. Using the Carman–Kozeny relation, we can then calculate the isotropic permeability K from*

$$K = \frac{1}{72\tau}\frac{\phi^3 d_p^2}{(1-\phi)^2},$$

where we further assume that $\tau = 0.81$. Then, petrophysical parameters can be generated as follows (the resulting porosity field is shown in the left plot of Figure 3):

```
G = cartGrid([50 20]);
p = gaussianField(G.cartDims, [0.2 0.4], [11 3], 2.5); p = p(:);
rock.poro = p;
rock.perm = p.^3.*(1e−5)^2./(0.81*72*(1−p).^2);
```

Next, we will use the same Gaussian field methodology to generate layered realisations, for which the permeability in each geological layer is independent of *the other layers and log-normally distributed. Each layer can be represented by several grid cells in the vertical direction. Here, we generate a stratigraphic grid with wavy geological faces and a single fault and specify four geological layers with mean values of* 100 mD*,* 400 mD*,* 50 mD*, and* 350 mD *from top to bottom (stratigraphic grids are numbered from the top and downward)*

```
G = processGRDECL(simpleGrdecl([50 30 10], 0.12));
K = logNormLayers(G.cartDims, [100 400 50 350], 'indices', [1 2 5 7 11]);
```

The layers are represented with one, three, two, and four grid cells, respectively, in the vertical direction. The resulting permeability is shown in the right plot of Figure 3.

Using smoothed Gaussian fields to generate random petrophysical variables is, of course, a gross simplification of geostatistics. For more realistic distributions of petrophysical parameters, the reader should consider using e.g., GSLIB [11] or commercial software for geological modelling.

2.3 Discretisation of Flow Equations

To keep technical details at a minimum, we will in the following consider a simplified set of single-phase flow equations,

$$\nabla \cdot \vec{v} = q, \qquad \vec{v} = -\mathbf{K}\nabla p, \qquad \text{in } \Omega \subset \mathbb{R}^d. \tag{1}$$

Here, $\vec{v}$ denotes the Darcy velocity, p pressure, and $\mathbf{K}$ permeability. All external boundaries $\partial\Omega$ are equipped with either prescribed pressure (Dirichlet) or prescribed flux (Neumann) boundary conditions. Let $\boldsymbol{u}_i$ be the vector of outward fluxes of the faces of Ω_i and let p_i denote the pressure at the cell centre and $\boldsymbol{\pi}_i$ the face pressures. Discretisation methods used for reservoir simulation are constructed to be locally conservative and exact for linear solutions. Such schemes can be written in a form that relates these three quantities through a matrix $\boldsymbol{T}_i$ of one-sided transmissibilities,

$$\boldsymbol{u}_i = \boldsymbol{T}_i(\boldsymbol{e}_i p_i - \boldsymbol{\pi}_i), \qquad \boldsymbol{e}_i = (1, \ldots, 1)^\mathsf{T}. \tag{2}$$

Examples include the two-point flux-approximation method [6], the lowest-order mixed finite-element methods [7], multipoint flux approximation schemes [5, 13, 4], and recently developed mimetic finite-difference methods [8]. Two-point discretisations give diagonal transmissibility matrices and are not convergent for general grids. Mixed, multipoint, and mimetic methods are consistent and convergent on non-orthogonal grids, but lead to full matrices $\boldsymbol{T}_i$. Such schemes will be discussed in more detail in Section 3; for now we only assume that there exists a consistent scheme on the form (2) that is convergent for fully unstructured, polyhedral grids.

In the following, we only consider schemes that may be written in hybridised mixed form, although MRST also supports mixed forms. Note that this restriction, which excludes some multipoint schemes, is only imposed to ease the presentation and give a uniform formulation of a large class of schemes. The underlying principles may be applied to any reasonable scheme. By augmenting (2) with flux and pressure continuity across cell faces, we obtain the following linear system

$$\begin{bmatrix} \boldsymbol{B} & \boldsymbol{C} & \boldsymbol{D} \\ \boldsymbol{C}^{\mathsf{T}} & \boldsymbol{0} & \boldsymbol{0} \\ \boldsymbol{D}^{\mathsf{T}} & \boldsymbol{0} & \boldsymbol{0} \end{bmatrix} \begin{bmatrix} \boldsymbol{u} \\ -\boldsymbol{p} \\ \boldsymbol{\pi} \end{bmatrix} = \begin{bmatrix} \boldsymbol{0} \\ \boldsymbol{q} \\ \boldsymbol{0} \end{bmatrix}. \tag{3}$$

Here, the first row in the block-matrix equation corresponds to Darcy's law in the form (2) for all grid cells, the second row corresponds to mass conservation for all cells, whereas the third row expresses continuity of fluxes for all cell faces. Thus, $\boldsymbol{u}$ denotes the outward face fluxes ordered cell-wise (fluxes over interior faces and faults appear twice with opposite signs), $\boldsymbol{p}$ denotes the cell pressures, and $\boldsymbol{\pi}$ the face pressures. The matrices $\boldsymbol{B}$ and $\boldsymbol{C}$ are block diagonal with each block corresponding to a cell. For the two matrices, the i'th blocks are given as $\boldsymbol{T}_i^{-1}$ and $\boldsymbol{e}_i$, respectively. Similarly, each column of $\boldsymbol{D}$ corresponds to a unique face and has one (for boundary faces) or two (for interior faces) unit entries corresponding to the index(s) of the face in the cell-wise ordering.

The hybrid system (3) can be solved using a Schur-complement method and MATLAB's standard linear solvers or third-party linear system solver software such as AGMG [28]. A block-wise Gaussian elimination for (3) yields a positive-definite system (the Schur complement) for the face pressures,

$$\big(\boldsymbol{D}^{\mathsf{T}}\boldsymbol{B}^{-1}\boldsymbol{D} - \boldsymbol{F}^{\mathsf{T}}\boldsymbol{L}^{-1}\boldsymbol{F}\big)\boldsymbol{\pi} = \boldsymbol{F}^{\mathsf{T}}\boldsymbol{L}^{-1}\boldsymbol{q}, \tag{4}$$

where $\boldsymbol{F} = \boldsymbol{C}^{\mathsf{T}}\boldsymbol{B}^{-1}\boldsymbol{D}$ and $\boldsymbol{L} = \boldsymbol{C}^{\mathsf{T}}\boldsymbol{B}^{-1}\boldsymbol{C}$. Given the face pressures, the cell pressures and fluxes can be reconstructed by back-substition, i.e., solving

$$\boldsymbol{L}\boldsymbol{p} = \boldsymbol{q} + \boldsymbol{F}^{\mathsf{T}}\boldsymbol{\pi}, \qquad \boldsymbol{B}\boldsymbol{v} = \boldsymbol{C}\boldsymbol{p} - \boldsymbol{D}\boldsymbol{\pi}.$$

Here, the matrix $\boldsymbol{L}$ is by construction diagonal and computing fluxes is therefore an inexpensive operation. It is also worth noting that we only need $\boldsymbol{B}^{-1}$ in the solution procedure above. Many schemes—including the mimetic method, the MPFA-O method, and the standard two-point scheme—yield algebraic approximations for the $\boldsymbol{B}^{-1}$ matrix. Thus, (3) encompasses a family of discretisation schemes whose properties are determined by the choice of $\boldsymbol{B}$, which we will discuss in more detail in Section 3.1.

2.4 Putting it all Together

In this section, we will go through a very simple example to give an overview of how to set up and use a discretisation as introduced in the previous section to solve the single-phase pressure equation

$$\nabla \cdot \vec{v} = q, \qquad \vec{v} = -\frac{\mathsf{K}}{\mu}\big[\nabla p + \rho g \nabla z\big]. \tag{5}$$

First, we construct a Cartesian grid of size $n_x \times n_y \times n_z$ cells, where each cell has dimension $1 \times 1 \times 1$ m and set an isotropic and homogeneous permeability of 100 mD, a fluid viscosity of 1 cP, and a fluid density of 1014 kg/m^3:

```
nx = 20; ny = 20; nz = 10;
G = computeGeometry(cartGrid([nx, ny, nz]));
rock.perm = repmat(100 * milli*darcy, [G.cells.num, 1]);
fluid = initSingleFluid('mu', 1*centi*poise, 'rho', 1014*kilogram/meter^3);
gravity reset on
```

The simplest way to model inflow or outflow from the reservoir is to use a fluid source/sink. Here, we specify a source with flux rate of $1\,\mathrm{m}^3$/day in each grid cell.

```
c   = (nx/2*ny+nx/2 : nx*ny : nx*ny*nz) .';
src = addSource([], c, ones(size(c)) ./ day());
```

Flow solvers in MRST automatically assume no-flow conditions on all outer (and inner) boundaries; other types of boundary conditions need to be specified explicitly. To draw fluid out of the domain, we impose a Dirichlet boundary condition of $p = 10\,\mathrm{bar}$ at the global left-hand side of the model.

```
bc = pside([], G, 'LEFT', 10*barsa());
```

Here, the first argument has been left empty because this is the first boundary condition we prescribe. The left plot in Figure 4 shows the placement of boundary conditions and sources in the computational domain. Next, we construct the system components for the hybrid mimetic system (3), with a mimetic discretisation, based on input grid and rock properties.

```
S = computeMimeticIP(G, rock, 'Verbose', true);
```

Rather than storing $\boldsymbol{B}$, we store its inverse $\boldsymbol{B}^{-1}$. Similarly, the $\boldsymbol{C}$ and $\boldsymbol{D}$ blocks are not represented in the S structure; they can easily be formed explicitly whenever needed, or their action can easily be computed.

Finally, we compute the solution to the flow equation. To this end, we must first create a state object that will be used to hold the solution and then pass this objects and the parameters to the incompressible flow solver.

```
rSol = initResSol(G, 0);
rSol = solveIncompFlow(rSol, G, S, fluid,'src', src, 'bc', bc);
p = convertTo(rSol.pressure(1:G.cells.num), barsa() );
```

Having computed the solution, we convert the result back to the unit bars. The right plot in Figure 4 shows the corresponding pressure distribution, where we clearly can see the effects of the boundary conditions, the source term, and gravity.

The same basic steps can be repeated on (almost) any type of grid; the only difference is placing the source terms and how to set the boundary conditions, which will typically be more complicated on a fully unstructured grid. We will come back with more examples later in the paper, but then we will not explicitly state all details of the corresponding MRST scripts. Before giving more

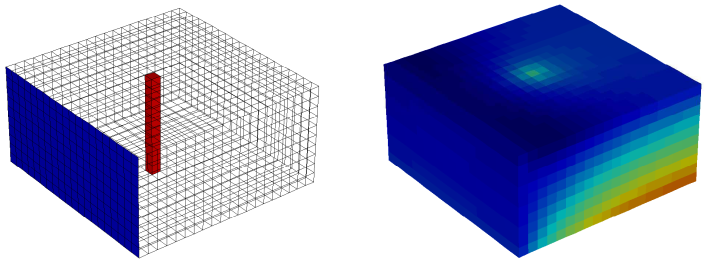

Figure 4: Example of a simple flow driven by a column of source cells and a Dirichlet boundary condition. The left plot shows the model setup and the right plot the corresponding pressure solution.

examples, however, we will introduce the multiscale flow solver implemented in MRST.

2.5 Multiscale Flow Simulation

Multiscale flow solvers [16, 14] can be seen as numerical methods that take a fine-scale model as input, but solve for a reduced set of unknowns defined on a coarse grid to produce a solution that has both coarse-scale and fine-scale resolution. A key characteristic with multiscale methods is that they incorporate fine-scale information into a set of coarse-scale equations in a way that is consistent with the local property of the differential operator. In an abstract formulation, a multiscale method uses two operators: a compression (or restriction) operator that takes information from the fine scale to the coarse scale, and a reconstruction (or prolongation) operator that takes information from the coarse scale to the fine scale. The compression operator is used to reduce the system of discretised flow equations on a fine grid to a system with significantly fewer unknowns defined on a coarse grid. Similarly, the reconstruction operator is used to construct an approximate fine-scale solution from the solution computed on the coarse scale. The reconstruction operators are typically computed numerically by solving a localised flow problem as in an upscaling method.

Different multiscale flow solvers are distinguished by how they define their degrees of freedom and the compression and reconstruction operators. In the multiscale finite-volume (MsFV) method [17, 31], the coarse-scale degrees-of-freedom are associated with pressure values at the vertexes of the coarse grid. The reconstruction operator is associated with pressure values and is defined by solving flow problems on a dual coarse grid. (In addition, the method needs to solve a local flow problem on the primal coarse grid to recover conservative fine-scale fluxes). In the multiscale mixed finite-element (MsMFE) method [9, 3], the coarse-scale degrees-of-freedom are associated with faces in the coarse grid (coarse-grid fluxes) and the reconstruction operator is associated with the fluxes and is defined by solving flow problems on a primal coarse grid. In the following, we will present the MsMFE method in more detail. To this end, we will use a finite-element formulation, but the resulting discrete method will have all the characteristics of a (mass-conservative) finite-volume method.

The multiscale method implemented in MRST is based on a hierarchical two-level grid in which the blocks Ω_i in the coarse simulation grid consist of a connected set of cells from the underlying fine grid, on which the full heterogeneity is represented. In its simplest form, the approximation space consists of a constant approximation of the pressure inside each coarse block and a set of velocity basis functions associated with each interface between two coarse blocks. Consider two neighbouring blocks Ω_i and Ω_j, and let Ω_{ij} be a neighbourhood containing Ω_i and Ω_j. The basis functions $\vec{\psi}_{ij}$ are constructed by solving

$$\vec{\psi}_{ij} = -\mathsf{K}\nabla p_{ij}, \qquad \nabla \cdot \vec{\psi}_{ij} = \begin{cases} w_i(x), & \text{if } x \in \Omega_i, \\ -w_j(x), & \text{if } x \in \Omega_j, \\ 0, & \text{otherwise}, \end{cases} \tag{6}$$

in Ω_{ij} with $\vec{\psi}_{ij} \cdot \vec{n} = 0$ on $\partial\Omega_{ij}$. If $\Omega_{ij} \neq \Omega_i \cup \Omega_j$, we say that the basis function is computed using overlap or oversampling. The purpose of the weighting function $w_i(x)$ is to distribute the divergence of the velocity, $\nabla \cdot \vec{v}$, over the block and produce a flow with unit flux over the interface $\partial\Omega_i \cap \partial\Omega_j$, and the function is therefore normalised such that its integral over Ω_i equals one. Alternatively, the method can be formulated on a single grid block Ω_i by specifying a flux distribution (with unit average) on one face and no-flow condition on the other faces, see [1] for more details. In either case, the multiscale basis functions—represented as vectors Ψ_{ij} of fluxes—are then collected as columns in a matrix $\boldsymbol{\Psi}$, which will be our reconstruction operator for fine-scale fluxes. To define the compression operator, we introduce two prolongation operators $\boldsymbol{\mathcal{I}}$ and $\boldsymbol{\mathcal{J}}$ from blocks to cells and from coarse interfaces to fine faces, respectively. The operator $\boldsymbol{\mathcal{I}}$ is defined such that element ij equals one if block number j contains cell number i and zero otherwise; $\boldsymbol{\mathcal{J}}$ is defined analogously. The transposed of these operators will thus correspond to the sum over all fine cells of a coarse block and all fine-cell faces that are part of the faces of the coarse blocks. Applying these compression operators and $\boldsymbol{\Psi}^\mathsf{T}$ to the fine-scale system, we obtain the following global coarse-scale system

$$\begin{bmatrix} \boldsymbol{\Psi}^\mathsf{T}\boldsymbol{B}\boldsymbol{\Psi} & \boldsymbol{\Psi}^\mathsf{T}\boldsymbol{C}\boldsymbol{\mathcal{I}} & \boldsymbol{\Psi}^\mathsf{T}\boldsymbol{D}\boldsymbol{\mathcal{J}} \\ \boldsymbol{\mathcal{I}}^\mathsf{T}\boldsymbol{C}^\mathsf{T}\boldsymbol{\Psi} & \mathbf{0} & \mathbf{0} \\ \boldsymbol{\mathcal{J}}^\mathsf{T}\boldsymbol{D}^\mathsf{T}\boldsymbol{\Psi} & \mathbf{0} & \mathbf{0} \end{bmatrix} \begin{bmatrix} \boldsymbol{u}^c \\ -\boldsymbol{p}^c \\ \boldsymbol{\pi}^c \end{bmatrix} = \begin{bmatrix} \mathbf{0} \\ \boldsymbol{\mathcal{I}}^\mathsf{T}\boldsymbol{q} \\ \mathbf{0} \end{bmatrix}. \tag{7}$$

Once (7) is solved, the fine-scale fluxes can be obtained immediately as $\boldsymbol{v} = \boldsymbol{\Psi}\boldsymbol{u}^c$. The basic steps of the multiscale algorithm are summarised in Figure 5. More details about how to include wells in a appropriate way is given in [30].

Having introduced the multiscale method, we should explain how to use it. To this end, we consider a simple example.

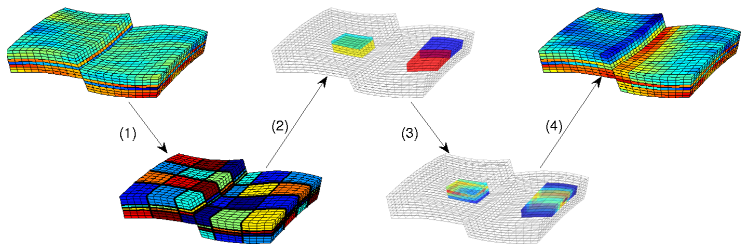

Figure 5: Key steps of the multiscale method: (1) blocks in the coarse grid are defined as connected collections of cells from the fine grid; (2) a local flow problem is defined for all pairs of blocks sharing a common face; (3) the local flow problems are solved and the solutions are collected as basis functions (reconstruction operators); and (4) the global coarse-system (7) is assembled and solved, then a fine-scale solution can be reconstructed.

Example 2 (Log-Normal Layered Permeability) *In this example, we will revisit the setup from the previous section. However, we neglect gravity and instead of assuming a homogeneous permeability, we increase the number of cells in the vertical direction to 20, impose a log-normal, layered permeability as shown in Figure 3, and use the layering from the permeability to determine the extent of the coarse blocks; a large number of numerical experiments have shown that the MsMFE method gives best resolution when the coarse blocks follow geological layers [3]. In MRST, this amounts to:*

```
[K, L] = logNormLayers([nx, ny, nz], [200 45 350 25 150 300], 'sigma', 1);
:
p = processPartition(G, partitionLayers(G, [Nx, Ny], L) );
:
plotCellData(G,mod(p,2));
outlineCoarseGrid(G,p,'LineWidth',3);
```

The permeability and the coarse grid are shown in Figure 6. Having partitioned the grid, the next step is to build the grid structure for the coarse grid and generate and solve the coarse-grid system.

```
CG = generateCoarseGrid(G, p);
CS = generateCoarseSystem(G, rock, S, CG, ...
       ones([G.cells.num, 1]),'bc', bc, 'src', src);
xMs  = solveIncompFlowMS(initResSol(G, 0.0), G, CG, ...
       p, S, CS, fluid,'src', src, 'bc', bc);
```

The multiscale pressure solution is compared to the corresponding fine-scale solution in Figure 6. The solutions appear to be quite close in the visual norm.

For single-phase problems, a multiscale flow solver without any form of parallelism will have a computational cost that is comparable to that of a fine-scale flow solver equipped with an efficient linear routine, i.e., MATLAB's built-in solvers for small problems and e.g., the AGMG solver [28] for large problems.

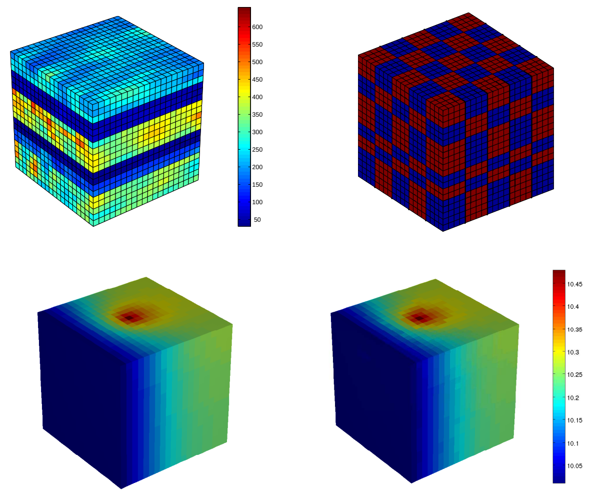

Figure 6: Comparison of the MsMFE and fine-scale mimetic flow solvers for the setup from Figure 4. The top plots show the layered permeability field and the corresponding partitioning into coarse blocks. The lower plots show the fine-scale pressure solution (left) and the multiscale solution (right).

The advantage of a multiscale solver comes first when considering multiphase flow problems, as we will discuss in the next section.

2.6 Two-Phase Flow

Two-phase incompressible flow of a wetting and non-wetting fluid can be described by the following system of equations:

$$\nabla \cdot \vec{v} = q, \qquad \vec{v} = -\mathbf{K}\big[\lambda \nabla p + (\lambda_w \rho_w + \lambda_n \rho_n) g \nabla z\big], \tag{8}$$

$$\phi \frac{\partial s_w}{\partial t} + \nabla \cdot \Big(f_w(s_w)\big[\vec{v} + \lambda_n(\rho_n - \rho_w) g \mathbf{K} \nabla z\big]\Big) = q_w. \tag{9}$$

Here, ρ_α denotes the density, λ_α the mobility, and $f_\alpha = \lambda_\alpha/\lambda$ the fractional flow of phase α, where $\lambda = \lambda_n + \lambda_w$ is the total mobility. The industry-standard approach is to use implicit discretisations and solve (8)–(9) as a fully-coupled system. In MRST, on the other hand, our goal has been to obtain maximum flexibility in combining different types of solvers. Hence, the toolbox assumes a sequential solution strategy: First, (8) is solved with fixed saturation values to provide pressure and fluxes, and then the fluxes are used to evolve the saturations according to (9). If necessary, the two steps can be iterated until convergence in a suitable norm.

All flow solvers in MRST are fully applicable to the two-phase flow equation (8), except for the MsMFE method, which does not support gravity in the current release of MRST. On the other hand, multiscale flow solvers are developed mainly to be efficient for multiphase problems, and in particular for two-phase incompressible equations, where the key to computational efficiency is reuse of previous computations. For a multiphase system, the basis functions will become time-dependent when K is replaced by $\lambda\mathsf{K}$ in (6), but this time-dependence is weak for an incompressible system, and the basis functions can therefore be computed initially and updated infrequently throughout a simulation. Solving the coarse-scale problem (7) is usually inexpensive compared to solving the corresponding fine-scale system or computing basis functions.

MRST supports two basic saturation solvers that both use a single-point upwind discretisation. Dropping subscripts to denote phases and assuming no gravity, they can be written in the form

$$\begin{aligned} s_i^{n+1} = s_i^n + \frac{\Delta t}{\phi_i|c_i|}\Big(\max(q_i,0) + f(s_i^m)\min(q_i,0)\Big) \\ - \frac{\Delta t}{\phi_i|c_i|}\Big(\sum_j\big[f(s_i^m)\max(v_{ij},0) + f(s_j^m)\min(v_{ij},0)\big]\Big), \qquad (10) \end{aligned}$$

Here, s_i is the average saturation in grid cell c_i, v_{ij} denotes the flux over the face between cells i and j. For $m = n$, the scheme is explicit, whereas for $m = n+1$, we obtain an implicit scheme that is solved by a Newton–Raphson method. For systems with gravity forces, MRST uses standard upstream mobility weighing; that is, the upwind direction is determined independently for each phase using the phase velocities $\vec{v}_\alpha$.

The observant reader may have noticed that the capillary pressure is missing in our two-phase model. In (8), capillary effects can be included by defining the pressure as the *global* pressure, $p = p_n - p_c$, where the so-called complementary pressure is defined through the relation $\nabla p_c = f_w\nabla(p_n - p_w)$.

So far, the paper has given a quick overview of the basic functionality and solvers in MRST Release 2010a. In the next section, we will go into more details about consistent and convergent discretisations on unstructured polyhedral grids, before we end the paper with an overview of how the resulting solvers can be applied to more advanced examples, including solvers and functionality that are not yet released publicly.

3 Mimetic Discretisation Methods

In this section we will discuss the mimetic method in more detail. We start by discussing the inner product, which can be used to design the properties of the method. Then we give a short discussion of Peacemann-type well models for the method.

3.1 Inner Products

The mimetic method (see [8]) is defined in terms of an inner product $\boldsymbol{M}$ or equivalently an inverse inner product $\boldsymbol{T}$. As we have seen above, the system (3) can be reduced to a linear equation that only involves the face pressures

$\boldsymbol{\pi}$, using a transformation that requires the computation of $\boldsymbol{B}^{-1}$. In this case, only an inverse inner product is needed. In the following, we describe a few inner products (and inverse inner products) while emphasising aspects of implementation and discuss specific properties of the different discretisations. The implementation can be found in `computeMimeticIP.m` in MRST [25].

In the original method [8], inner products of discrete velocities are considered. In reservoir simulation however, it is more common to consider the face fluxes as unknowns. Accordingly, we will consider inner products of fluxes rather than velocities. We note here that the relation between the two is trivial, as an inner product of velocities becomes an inner product for fluxes by pre- and post-multiplying by the inverse area of the corresponding faces. Let $\boldsymbol{A}$ be the diagonal matrix with a_{ii} the face area of the i-th face. Then the flux inner product $\boldsymbol{M}_{\text{flux}}$ is related to the velocity inner product $\boldsymbol{M}_{\text{vel}}$ through

$$\boldsymbol{M}_{\text{flux}} = \boldsymbol{A}^{-1}\boldsymbol{M}_{\text{vel}}\boldsymbol{A}^{-1}. \tag{11}$$

Henceforth we will only consider inner products for fluxes.

To yield a consistent discretisation of (1), an inner product matrix $\boldsymbol{M}$ or an inverse inner product $\boldsymbol{T}$ must result in a discretisation which is exact for linear pressures. This condition can be written as

$$\begin{aligned} \boldsymbol{MNK} &= \boldsymbol{C}, \\ \boldsymbol{NK} &= \boldsymbol{TC}, \end{aligned} \tag{12}$$

where each row $\vec{c}_i^{\mathsf{T}}$ of the matrix $\boldsymbol{C}$ is the vector pointing from the cell centroid to the corresponding face centroid, and each row $\vec{n}_i^{\mathsf{T}}$ of $\boldsymbol{N}$ is the area weighted normal vector. Furthermore, the inner product matrix must be positive definite. Any inner product fulfilling these requirements (see [8] for the discrete flux case) can be represented in the form

$$\boldsymbol{M} = \frac{1}{|\Omega_i|}\boldsymbol{CK}^{-1}\boldsymbol{C}^{\mathsf{T}} + \boldsymbol{Q}_N^{\perp}{}^{\mathsf{T}}\boldsymbol{S}_M\boldsymbol{Q}_N^{\perp}, \tag{13}$$

where $\boldsymbol{Q}_N^{\perp}$ is an orthonormal basis for the null space of $\boldsymbol{N}^{\mathsf{T}}$, and $\boldsymbol{S}_M$ is any positive definite matrix. In the code and the following examples, we use a null space projection $\boldsymbol{P}_N^{\perp} = \boldsymbol{Q}_N^{\perp}\boldsymbol{S}_M\boldsymbol{Q}_N^{\perp} = \boldsymbol{I} - \boldsymbol{Q}_N\boldsymbol{Q}_N{}^{\mathsf{T}}$ where $\boldsymbol{Q}_N$ is a basis for the space spanned by the columns of $\boldsymbol{N}$. Similarly, the inverse inner products take the form

$$\boldsymbol{T} = \frac{1}{|\Omega_i|}\boldsymbol{NKN}^{\mathsf{T}} + \boldsymbol{Q}_C^{\perp}{}^{\mathsf{T}}\boldsymbol{S}\boldsymbol{Q}_C^{\perp}. \tag{14}$$

We will now outline a few specific choices that are implemented in MRST.

IP_SIMPLE. In MRST the default inner product reads

$$\begin{aligned} \boldsymbol{Q} &= \operatorname{orth}(\boldsymbol{A}^{-1}\boldsymbol{N}) \\ \boldsymbol{M} &= \frac{1}{|\Omega_i|}\boldsymbol{CK}^{-1}\boldsymbol{C}^{\mathsf{T}} + \frac{d|\Omega_i|}{6\,\operatorname{tr}(\boldsymbol{K})}\boldsymbol{A}^{-1}(\boldsymbol{I} - \boldsymbol{QQ}^{\mathsf{T}})\boldsymbol{A}^{-1} \end{aligned} \tag{15}$$

with the approximate inverse

$$\begin{aligned} \boldsymbol{Q} &= \operatorname{orth}(\boldsymbol{AC}) \\ \boldsymbol{T} &= \frac{1}{|\Omega_i|}\Big[\boldsymbol{NKN}^\mathsf{T} + \frac{6}{d}\operatorname{tr}(\boldsymbol{K})\boldsymbol{A}(\boldsymbol{I}-\boldsymbol{QQ}^\mathsf{T})\boldsymbol{A}\Big]. \end{aligned} \tag{16}$$

This inner product was used in [3] inspired by [8] and was chosen to resemble the the mixed Raviart–Thomas inner product (they are equal for scalar permeability on orthogonal grids). Since this inner product is based on velocities, the pre- and post-multiplication of (inverse) face areas appear, and it might not be obvious that it fits into the formulations (13)–(14). However, after a small computation one is convinced that the second part of (13) is invariant under multiplication by $\boldsymbol{P}_N^\perp$ so its eigenspace corresponding to the non-zero eigenvalues must be equal to the nullspace of $\boldsymbol{N}^\mathsf{T}$. A similar argument holds for the inverse inner product.

Two-point and related. The TPFA method is the gold standard for practical reservoir simulation despite its theoretical shortcomings. Since the TPFA requires a diagonal tensor, it is easily seen from (12) that this is only possible in the case when the vectors $\boldsymbol{K}\vec{n}_i$ and $\vec{c}_i$ are parallel, i.e., the grid is K-orthogonal. In any case (K-orthogonality or not), we define the diagonal TPFA transmissibility tensor $\boldsymbol{T}$ by

$$\boldsymbol{T}_{ii} = \vec{n}_i \cdot \boldsymbol{K}\vec{c}_i/|\vec{c}_i|^2. \tag{17}$$

This defines the unique TPFA method for K-orthogonal grids; the extension to non-orthogonal grids is not unique, however, since the TPFA method does not give a consistent discretisation in this case. Because of its simplicity, the TPFA method is strictly monotone, which implies that the fluxes form a directed acyclic graph, a property that can be used to accelerate the solution of the transport equations considerably, as discussed in [27].

When written in its standard form, the TPFA method is cell-centred and thus less computationally costly than face-centred methods that arise from a consistent hybrid mimetic formulation. However, since the method is not consistent, it will in many cases be necessary to investigate the grid-orientation effects of the TPFA method before using it for realistic simulations. We therefore present a mimetic-type discretisation that coincides with the TPFA method in its region of validity, while at the same time giving a valid mimetic inner product for all types of grids and permeability tensors. This minimises the need for investigating other effects of the TPFA method, such as errors introduced by corners and well modelling. An advantage of this method compared to using, e.g., an MPFA method is that the implementation is simpler for general unstructured grids. We call the corresponding method IP_QTPFA and it is defined by

$$\begin{aligned} \boldsymbol{T} &= \frac{1}{|\Omega_i|}\Big[\boldsymbol{NKN}^\mathsf{T} + 2\,\boldsymbol{P}_C^\perp \operatorname{diag}(\boldsymbol{NKN}^\mathsf{T})\boldsymbol{P}_C^\perp\Big], \\ \boldsymbol{M} &= \boldsymbol{T}^{-1}. \end{aligned} \tag{18}$$

We emphasise that this inner product evidently is invariant under coordinate transformations, but will only be diagonal for K-orthogonal grids.

Raviart–Thomas. Equation (1) is invariant when space and permeability are transformed as $\vec{x} \mapsto \boldsymbol{A}\vec{x}$ and $\mathsf{K} \mapsto \boldsymbol{A}^\mathsf{T}\mathsf{K}\boldsymbol{A}$, respectively. Because the inner product (15) uses the trace of $\boldsymbol{K}$ as a scaling factor, it will not be invariant under such transformations, since the trace of a matrix is only invariant under similarity transformations, i.e., $\mathrm{tr}(\boldsymbol{A}\boldsymbol{K}\boldsymbol{A}^{-1}) = \mathrm{tr}(\boldsymbol{K})$. However, we note that for orthogonal transformations we have $\boldsymbol{A}^{-1} = \boldsymbol{A}^\mathsf{T}$.

To eliminate the transformation dependency of IP_SIMPLE we introduce an inner product that is equivalent to the mixed Raviart–Thomas inner product for grids that are orthogonal and has the same principal axes as the permeability tensor

$$\boldsymbol{M} = \frac{1}{|\Omega_1|}\boldsymbol{C}\boldsymbol{K}\boldsymbol{C}^\mathsf{T} + \frac{|\Omega_i|}{6}\boldsymbol{P}_N^\perp\big[\mathrm{diag}(\boldsymbol{N}\boldsymbol{K}\boldsymbol{N}^\mathsf{T})\big]^{-1}\boldsymbol{P}_N^\perp. \tag{19}$$

We call this inner product for IP_QRT. The corresponding quasi-inverse, which is the exact inverse for orthogonal grids, reads

$$\boldsymbol{T} = \frac{1}{|\Omega_i|}\Big[\boldsymbol{N}\boldsymbol{K}\boldsymbol{N}^\mathsf{T} + 6\,\boldsymbol{P}_C^\perp\,\mathrm{diag}(\boldsymbol{N}\boldsymbol{K}\boldsymbol{N}^\mathsf{T})\boldsymbol{P}_C^\perp\Big]. \tag{20}$$

This inner product will also, by the transformation property, be equal to the Raviart–Thomas formulation for all cases that can be transformed to the above case by an affine transformation. Using a mimetic inner product which is simpler to calculate and equal to the mixed Raviart–Thomas inner product for all grid cells is not possible because of the need to integrate the nonlinear function introduced by the determinant of the Jacobian of the mapping from the grid cell to the unit cell, in which the Raviart–Thomas basis functions are defined.

Local-flux mimetic MPFA. In addition to the above methods, which are all based on the assumption of a positive-definite inner product and exactness for linear flow, the MPFA method can be formulated as a mimetic method. This was first done by [20, 23] and is called the local-flux mimetic formulation of the MPFA method. In this case, all faces of a cell are such that each corner is associated with d unique faces, where d is the dimension. The inner product of the local-flux mimetic method gives exact result for linear flow and is block diagonal with respect to the faces corresponding to each corner of the cell, but it is not symmetric. The block-diagonal property makes it possible to reduce the system into a cell-centred discretisation for the cell pressures. This naturally leads to a method for calculating the MPFA transmissibilities. The crucial point is to have the corner geometry in the grid structure and handle the problems with corners which do not have three unique half faces associated. Currently the MPFA-O method is formulated in such a way [20] and work has been done for the MPFA-L method, but in this case the inner product will vary over the different corners.

We notice the the inner products IP_QTPFA in (18) and IP_QRT in (20) only differ by a constant in front of the regularisation part (the second term).

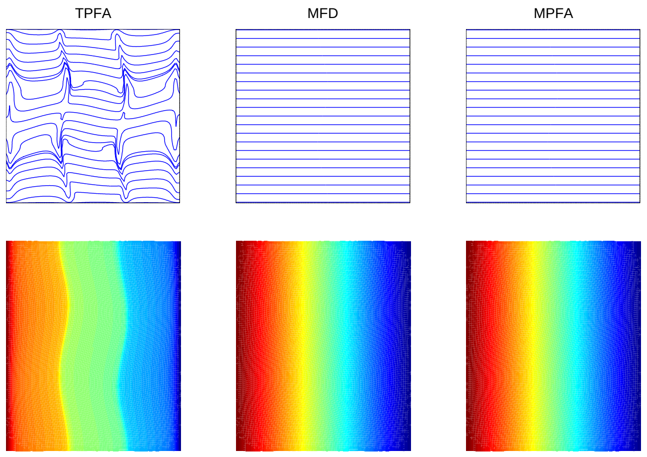

Figure 7: Grid-orientation effects for a homogeneous domain with Dirichlet boundary conditions (left,right) and no-flow conditions (top, bottom) computed with three different pressure solvers in MRST. The permeability field is homogeneous with anisotropy ratio 1 : 1000 aligned with the grid. The upper row shows streamlines visualizing the velocity field, whereas the bottom row shows the pressure field.

Both methods belong to a family whose inverse inner product can be written in the form

$$\begin{aligned} \boldsymbol{T} &= \frac{1}{|\Omega_i|}\Big[\boldsymbol{N}\boldsymbol{K}\boldsymbol{N}^{\mathsf{T}} + t\,\boldsymbol{P}_C^{\perp}\operatorname{diag}(\boldsymbol{N}\boldsymbol{K}\boldsymbol{N}^{\mathsf{T}})\boldsymbol{P}_C^{\perp}\Big] \\ \boldsymbol{M} &= \boldsymbol{T}^{-1}, \end{aligned} \tag{21}$$

where t is a parameter that can be varied continuously from zero to infinity.

Example 3 (Grid-Orientation Effects and Monotonicity) *It is well known that two-point approximations are convergent only in the special case of K-orthogonal grids. Mimetic and multipoint schemes, on the other hand, are constructed to be consistent and convergent for rough grids and full-tensor permeabilities, but may suffer from pressure oscillations for full-tensor permeabilities and large anisotropy ratios and/or high aspect ratio grids. In this example, we use one of the example grids supplied with MRST to illustrate these two observations. The routine* `twister` *normalises all coordinates in a rectilinear grid to the interval $[0,1]$, then perturbs all interior points by adding $0.03\sin(\pi x)\sin(3\pi(y-1/2))$ to the x-coordinates and subtracting the same value from the y coordinate before transforming back to the original domain. This creates a non-orthogonal, but smoothly varying, logically Cartesian grid.*

To investigate grid-orientation effects, we impose a permeability tensor with anisotropy ratio $1 : 1000$ aligned with the x-axis and compute the flow resulting from a prescribed horizontal pressure drop and no-flow conditions on the top and bottom boundaries. Figure 7 shows pressure computed on a 100×100 grid by

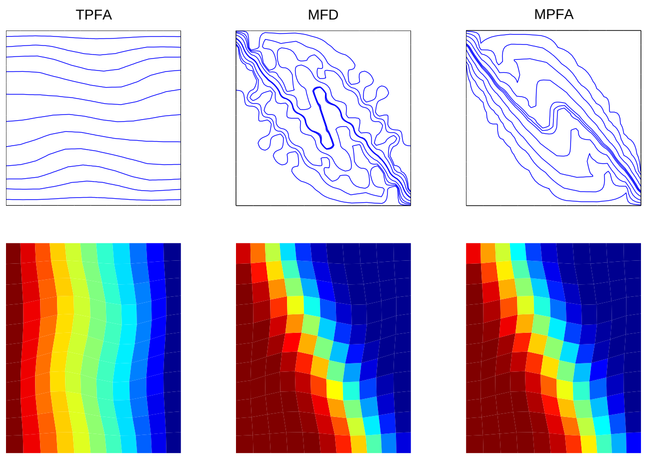

Figure 8: Monotonicity effects demonstrated with the same setup as in Figure 7, but with the anisotropy ratio 1 : 1000 making an angle $\pi/6$ with the grid directions.

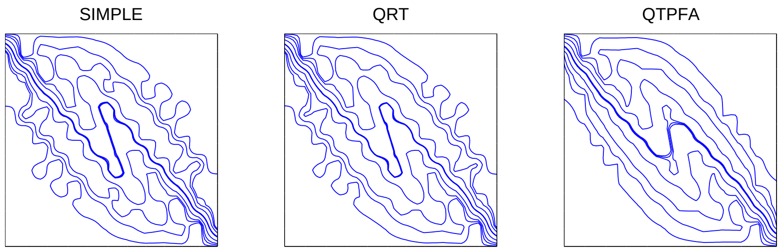

Figure 9: Lack of monotonicity visualised by tracing streamlines for the velocity fields computed by three mimetic pressure solvers in MRST for the same setup as in Figure 8.

the TPFA method, the mimetic method with inner product IP_SIMPLE, and the local-flux mimetic version of the MPFA-O method. To visualise the corresponding velocity field, we also show streamlines traced by MRST's implementation of Pollock's method. Whereas the mimetic and MPFA-O schemes produce the expected result, the pressure and velocity solutions computed by TPFA show significant grid-orientation effects and are obviously wrong.

In Figure 8, we have repeated the experiment with the tensor rotated by $\pi/6$ *on a grid with* 11×11 *cells. Again, we see that the solution computed by the TPFA scheme is wrong. In this case, the pressures computed with the mimetic and the MPFA-O schemes appear to be correct and have no discernible oscillations. However, the streamline distributions clearly show that the resulting velocity fields are highly oscillatory, in particular for the mimetic method with the IP_SIMPLE inner product. To compare the effect of using an approximate inverse in the inner-product matrices, we have computed the velocity field for the mimetic methods resulting from inner products* (16), (20), *and* (18). *From*

Table 1: Maximum error in cell pressure relative to maximum difference in cell-pressure for the family of inner products in Equation (21). The corresponding errors for the MPFA-O and the TPFA methods are 0.0074 and 0.035, respectively.

Inner product (t)	0.5	1	2	3	4
Error	0.0328	0.0202	0.0088	0.0074	0.0082
Inner product (t)	5	6	7	10	100
Error	0.00959	0.0106	0.0114	0.0129	0.0172

the streamline plots shown in Figure 9, it is evident that both IP_SIMPLE and IP_QRT yield more oscillatory velocity fields than the IP_QTPF method.

Example 4 (Real-Field Model) *In this example, we consider a synthetic 2D model derived from the 3D simulation model of a reservoir from offshore Norway. The original model is given as a* $46 \times 112 \times 22$ *logically Cartesian corner-point grid with 44,915 active cells. To assess grid-orientation effects introduced by different inner-products, we consider only the layer ten from the top of the model, which we flatten and modify so that the thickness of the layer is constant and all pillars in the corner-point description are vertical. Wells are assigned by keeping one perforation for some of the original wells. To generate a representative analytical solution, we model each well as a logarithmic singularity and set boundary conditions according to the solution obtained for the prescribed well pattern in an infinite reservoir,*

$$p(x, y) = \sum_i \frac{q_i}{2\pi K/\mu} \ln\Big(\sqrt{(x-x_i)^2 + (y-y_i)^2}\Big).$$

Figure 10 shows the pressure and the corresponding relative error for the IP_QRT method, as well as the error for the TPFA method. With the consistent mimetic scheme, the error is localized around the wells, whereas it is up to 10 % and distributed all over the reservoir for the TPFA method. (The full 3D model has a much rougher geometry that contains pinch-outs, sloping faults, and eroded layers, which all will contributed to larger grid-orientation effects for inconsistent methods). Note that a well model can correct for errors in the vicinity of the well, but not global errors as in the inconsistent TPFA method.

In Table 1 we report the maximum relative error in pressure for various members of the inner-product family introduced above. For this particular grid, the minimum error occurs around $t = 3$*, which is a method somewhere between the quasi-two-point and the quasi-Raviart–Thomas methods. The minimal error is similar to the error of the MPFA-O method.*

3.2 Finite Difference Stencils

To complete the discussion of the previously presented mimetic finite difference methods we demonstrate a few of the resulting finite difference stencils that relate the interface pressure values in (4). In particular, we discretise the pressure

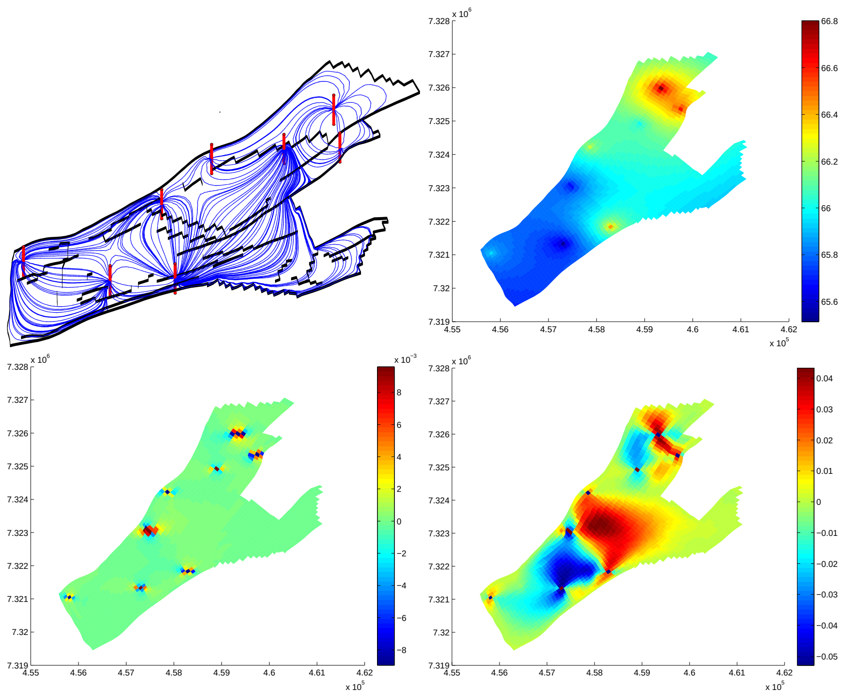
Figure 10: Grid-orientation errors on a 2D cartoon of a real-field model. The upper-left plot shows wells and streamlines tracing flow paths, the upper-right plot shows the pressure field computed by the IP_QRT inner product, the lower-left plot shows the corresponding relative error, whereas the lower-right plot shows the error for the TPFA method.

equation (1) with permeability $\mathsf{K} = I$ on a two-dimensional, equidistant grid, $\Delta x = \Delta y = 1$ using inner products already implemented in MRST. Figure 11 shows the results. We notice in particular that the 'IP_SIMPLE' inner product of equation (16) and the 'IP_QRT' inner product of equation (21) with parameter $t = 6$ produce stencils that have both positive and negative off-diagonal coupling terms. Moreover, setting $t = 4$ produces a stencil that resembles the classical five-point discretisation scheme of the Laplace operator on a rotated grid. Finally, if $t \in (2, 4)$, all off-diagonal coupling terms are negative.

3.3 Well Modelling

Wells in reservoirs typically have small diameters compared to the size of the simulation cells, and it is therefore common to employ a well index (productivity index) WI to relate the local flow rate q to the difference between the well pressure p_w and numerically computed pressure p_E in the perforated grid-cell as follows

$$-q = \lambda_t(s_E)\mathrm{WI}(p_E - p_w). \tag{22}$$

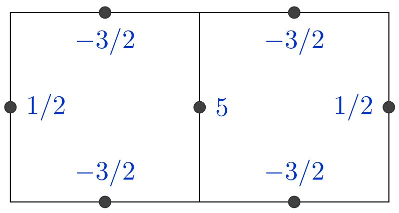

(a) IP_SIMPLE, IP_QRT($t = 6$)

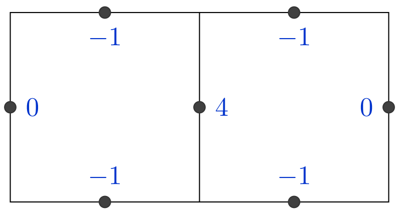

(b) IP_QRT($t = 4$)

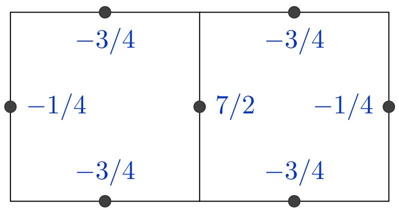

(c) IP_QRT($t = 3$)

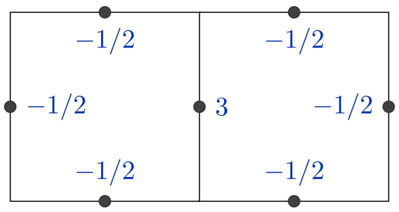

(d) IP_TPF, IP_QRT($t = 2$)

Figure 11: Finite difference stencils for interface pressures when $\Delta x = \Delta y = 1$ and $\mathbf{K} = I$.

Commonly used is Peaceman's well index [29], which for a vertical well in a Cartesian cell with dimensions $\Delta x \times \Delta y \times \Delta z$ is given as

$$\mathrm{WI} = \frac{2\pi k \Delta z}{\ln(r_0/r_w)}. \tag{23}$$

For isotropic media, k is given by $\mathbf{K} = k\mathbf{I}$, and $r_0 = 0.14(\Delta x^2 + \Delta y^2)^{\frac{1}{2}}$. Here, r_0 is the *effective well-cell radius* and can be interpreted as the radius at which the actual pressure equals the numerically computed pressure. The validity of the Peaceman well-index decreases rapidly with increasing near-well heterogeneity and grid skewness. It is also important to note that the Peaceman well-index is developed for the TPFA method and is not valid for other methods (such as MFE method with exact integration or mimetic methods in general) because different numerical methods in general give different well-block pressures. We will now give a short description of how to extend Peaceman's results to other methods than TPFA; for a more extensive study of well models, we refer to [22].

Assuming steady-state, single-phase, horizontal flow in a homogeneous and isotropic reservoir with radial flow near the well, there exists an analytical flow model near the well given by

$$p(r) = \frac{q\mu}{2\pi k \Delta z} \ln\Big(\frac{r}{r_w}\Big) + p_w. \tag{24}$$

We refer to [26, pages 150–153] for a derivation of this expression. Peaceman used the five-spot pattern problem to derive both numerical and analytical expressions for r_0 based on the relation above. However, the equivalent radius can also be calculated by simulating an infinite reservoir with one well and radial

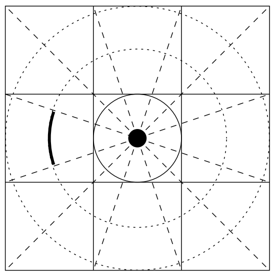
Figure 12: Section of infinite reservoir with well and radial flow.

Table 2: The constant $C(\beta)$ in the formula (25) for equivalent well radius for mimetic methods as a function of the aspect ratio β of the well block.

Inner product (β)	1	2	4	8	16	32	64
IP_SIMPLE	0.2926	0.2782	0.2520	0.2317	0.2198	0.2133	0.2100

flow, and we employ this method to calculate new equivalent radii for mimetic methods.

The radial flow simulation is done by forcing appropriate flux boundary conditions. Consider a section of the reservoir containing a well as displayed in Figure 12, we set $F_i = q\theta_i/2\pi$ as flux boundary conditions on a face i. When the resulting system is solved for pressure and flow, we use the analytical pressure relation (24) to compute a numerical equivalent radius r_0 from the pressure values in the well-block and on one boundary face.

If we assume that the equivalent radius for mimetic methods is on the same form as for TPFA shown above, then r_0 will depend on the actual inner product and the grid aspect ratio of the well block, $\beta = \Delta x/\Delta y$, i.e,

$$r_0(\mathrm{IP}, \beta) = C(\mathrm{IP}, \beta)(\Delta x^2 + \Delta y^2)^{\frac{1}{2}}. \tag{25}$$

The constant C is given in Table 2 for selected β for the IP_SIMPLE inner product.

4 Advanced Examples

A main purpose of MRST is to provide an efficient toolkit for the development and testing of new ideas. In this section, we present examples in which the solvers described in the previous sections are applied to more advanced examples. We will also show examples of solvers and functionality that have not yet been publicly released.

Given the importance of grid geometry on the quality of numerical computations, it is crucial to have flexible tools that allow testing algorithms on

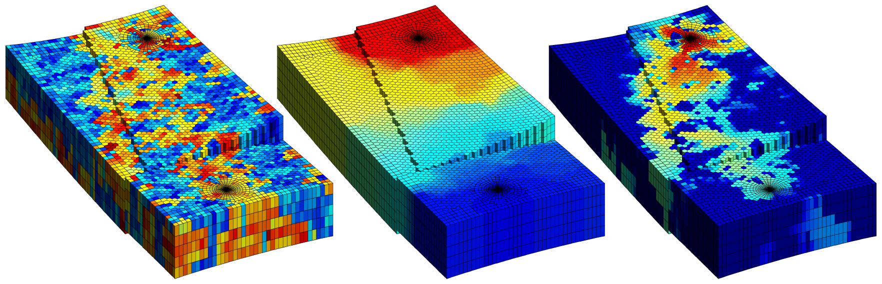

Figure 13: Two-phase flow computed on a pillar grid constructed by extruding an areal grid consisting of structured and unstructured parts: a radially refined grid, a Cartesian grid along the outer boundary, a hexahedral grid in the interior, and general polyhedral cells to glue everything together. The plots show permeability (left), pressure field (middle), and water saturation after 5000 days.

many different types of grids. In the first example, we highlight the ability to construct unstructured grids with complex connectivity and local refinement.

Example 5 (Flexible Gridding) *In this example we construct a constrained Voronoi grid from an initial distribution of points. Using the built-in* MATLAB *command* `voronoin`*, it is possible to construct uniform grids from uniform distributions of points. We extrude an unstructured areal grid with* 4509 *cells to a faulted model with* 5 *layers. The areal grid consists of three parts: A Cartesian grid at the outer boundary, a hexahedral grid in the interior, and a radial grid with exponential radial refinement around the wells. The radial grids is refined to an inner radius of* 0.3 m.

As in the standard corner-point grid format, the extrusion process is accomplished by assigning pillars to each node in the areal grid. Each volumetric cell in the extruded grid is given a set of z-coordinates for each of the nodes. The x and y coordinates can be computed from the pillars associated with the cell.

To illustrate the use of this grid, we have sampled permeability and porosity from layers 40–44 *of Model 2 from the 10th SPE Comparative Solution Project [10]. The permeability field is shown on the left in Figure 13. The wells are modelled as Dirichlet boundaries with pressures set to* 200 bar *and* 100 bar*, respectively, and we compute the pressure and water saturation with a sequentially implicit scheme in time steps of* 50 *days using the mimetic flow solver. The oil-water viscosity ratio is* 10*. The pressure and water saturation are shown after* 5000 *days of injection in Figure 13.*

In the rest of this section, we will go through several examples taken from our ongoing research activities, in which MRST is used to simulate flow on polyhedral grids of varying complexity in 3D. By doing so, we hope to give the reader a taste of the utility of the toolbox. We start by a short example which demonstrates the applicability of the MsMFE method on unstructured grids in 3D. Although several of our papers have argued that the method can easily be

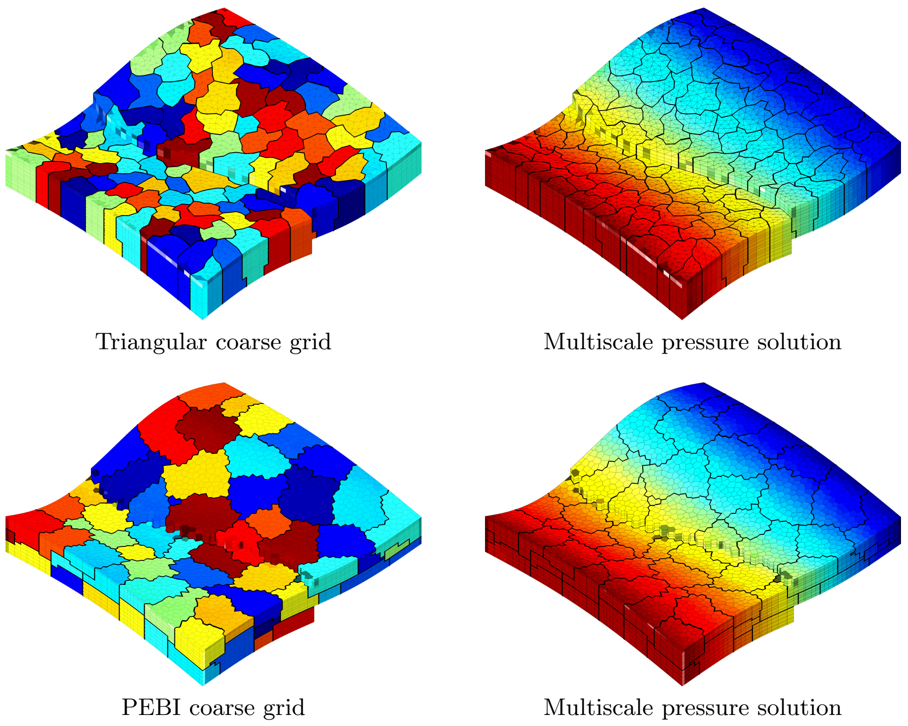

Figure 14: Multiscale discretisation of a flow problem with linear pressure drop on a triangular and a PEBI grid.

formulated on fully unstructured grids in 3D, the following is the first example demonstrating the actual capability on grids that do not have an underlying logically Cartesian structure.

Example 6 (Extruded Triangular and PEBI Grids) *The MsMFE method was previously demonstrated on Cartesian and logically Cartesian (corner-point) grids, see [2, 19, 3]. However, the method is equally feasible on general, unstructured grids provided there exists a suitable partitioning of the underlying (fine-scale) grid. Figure 14 shows the solution of the single-phase flow problem* (1) *with isotropic, homogeneous* $\mathbf{K}$ *on a computational domain* Ω *that has been discretised using both triangular and PEBI cells. These cells are subsequently partitioned into a coarse grid by means of the well-known software package METIS [18]. For simplicity, the PEBI grid was created as the Voronoi diagram of the triangular grid and hence the fault is more irregular on this grid. Despite the irregular block boundaries, the multiscale method is able to accurately capture the linear pressure drop from the west to the east boundaries on both grids.*

The public version of MRST currently supports single-phase and two-phase

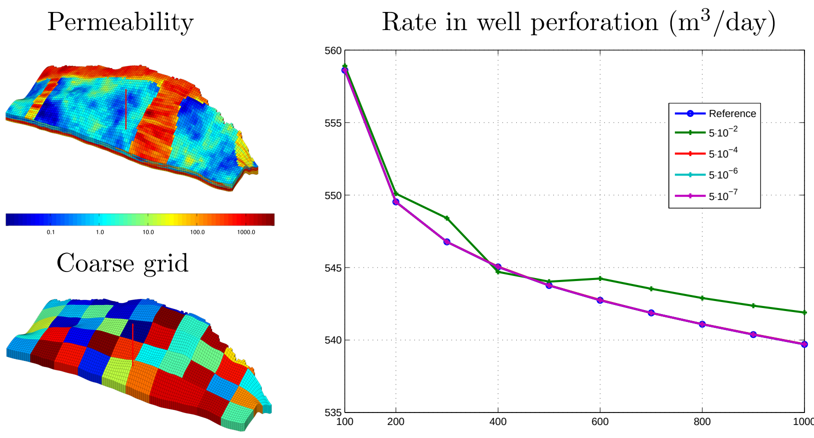

Figure 15: Primary production from a gas reservoir computed by the MsMFE method.

flow. Our in-house version of MRST has compressible black-oil fluid models implemented, along with several flow and transport solvers. In the last example, we will demonstrate the use of one of our experimental multiscale flow solvers to simulate compressible flow on a geological model with industry-standard complexity.

Example 7 (Primary Production from a Gas Reservoir) *In this example, we will briefly discuss the use of the MsMFE method to compute primary production from a gas reservoir. As our geological model, we will use one of the shallow-marine realisations from the SAIGUP study [24]. In our current in-house implementation of compressible black-oil models in the MsMFE method, compressibility is handled using a mixed residual formulation*

$$\begin{bmatrix} \boldsymbol{B} & \boldsymbol{C} \\ \boldsymbol{C}^{\mathsf{T}} & \boldsymbol{P} \end{bmatrix} \begin{bmatrix} \boldsymbol{u}_{\text{ms}} + \hat{\boldsymbol{u}}^{\nu+1} \\ \boldsymbol{p}_{\text{ms}} + \hat{\boldsymbol{p}}^{\nu+1} \end{bmatrix} = \begin{bmatrix} \boldsymbol{0} \\ \boldsymbol{P}\boldsymbol{p}^{n} + \boldsymbol{V}\boldsymbol{u}^{\nu} \end{bmatrix},$$

for which the elliptic multiscale basis functions act as predictors and a parabolic correction is computed using a standard (non)overlapping Schwarz domain-decomposition method. The method then iterates on the multiscale solution and the corrections until the fine-scale residual is below a prescribed tolerance. The geological model consists of $40 \times 120 \times 20$ *cells (see Figure 15) and is assumed to be initially filled with an ideal gas at* 200 bar *pressure. The reservoir is produced by a single producer, operating at a constant bottom-hole pressure of* 150 bar*. Figure 15 compares the fine-scale reference solution with multiscale solutions for different tolerances; as our measure, we have used the rate in the well perforation. Except for the coarsest tolerance,* $5 \cdot 10^{-2}$*, the multiscale solution appears to overlap with the fine-scale reference solution.*

Many reservoir management challenges can be cast as mathematical optimisation problems. Examples include data assimilation where a misfit function is to be minimised, and finding optimal well controls to maximise some economic performance measure. A popular approach to obtaining objective function gradients is the use of adjoint equations. The adjoint system of equations is the transpose of the linearised forward system, and accordingly has similar complexity as the forward simulation. Our in-house version of MRST includes an adjoint code for a sequential forward simulation using the mimetic discretization for the pressure equation and an implicit version of the scheme (9) for saturation. In addition, an adjoint code for the multiscale method combined with the flow based coarsening approach is included, see [21].

Example 8 (Optimising Net Present Value (NPV)) *In this example we consider a synthetic model with two horizontal injectors and one multilateral producer, see Figure 16. We attempt to maximise a simple NPV function; the oil revenue is \$100 per barrel and our costs are realised through water injection and production, each \$10 per barrel. This means that when the water cut in the producer exceeds* ≈ 0.82*, we are no longer making money. We compare three production strategies:*

1. *The producer operates at constant BHP until the water cut reaches* 0.82*, and the well is shut.*
2. *We assume that each producer well-segment is equipped with an inflow control device (ICD). The producer operates at constant BHP and whenever the water cut in a segment exceeds* 0.82*, the corresponding ICD shuts. The process is continued until all ICDs are shut.*
3. *We use the adjoint code to find optimal segment rates corresponding to a local maximum of the NPV-function.*

The initial simulation input is constant and equal rate for the two injectors and constant BHP for the producer. The initial simulation time is set to 500 *days which is equivalent to* $1.25\,\mathrm{PVI}$*. In Figure 16 we show the accumulated NPV for the three production scenarios. We observe that for production scenario 1, the well is shut down after about* 225 *days with an achieved NPV of \$* 72.8 *million. Scenario 2 is equal to scenario 1 until the first ICD is shut, and the improvement obtained by being able to shut down individual segments of the well is evident. All ICDs are shut after about 375 days, and the obtained NPV is \$* 79.9 *million. Finally, in scenario 3, water cut is not taken into account, only maximising the NPV. The obtained NPV is \$* 92.6 *million.*

5 Outlook

Replicablility is a fundamental scientific principle that is currently receiving increasing attention among computational scientists. The level of sophistication and complexity in new computational methods makes it difficult for researchers to implement methods published by others and replicate their results.

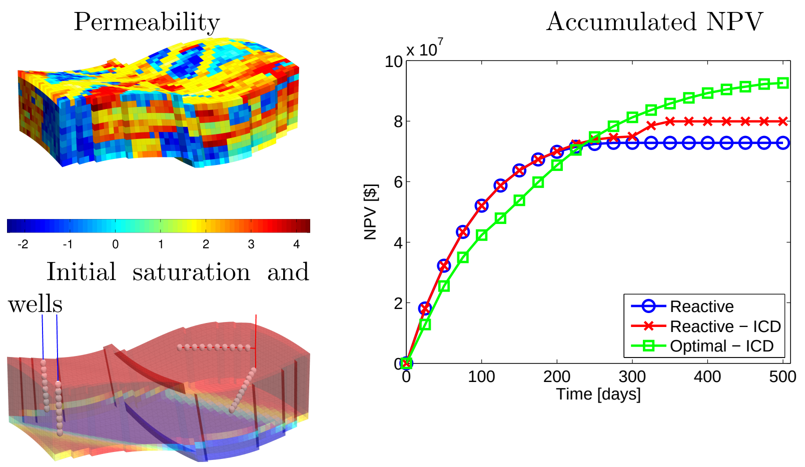

Figure 16: Accumulated net present value for the three production strategies.

We believe that releasing the MATLAB Reservoir Simulation Toolbox (MRST) under the GNU General Public License (GPL) is an important step for our group towards supporting the idea of reproducible science, thereby allowing others to more easily benefit from our efforts. In this paper we have given an overview of MRST and discussed in detail a family of consistent methods that are convergent on fully unstructured, polyhedral grids. We have also demonstrated the compressible black-oil and adjoint multiscale features that currently exists only in our in-house, development version of the package. Although we are not yet there, we are aiming towards a state where our publications on new computational methodologies can be accompanied by open-access software that can be used by others to verify our computational results.

6 Acknowledgements

The research was funded in part by the Research Council of Norway through grants no. 158908, 174551, 175962, 178013, and 186935.

References

[1] Aarnes, J.E., Kippe, V., Lie, K.A.: Mixed multiscale finite elements and streamline methods for reservoir simulation of large geomodels. Adv. Water Resour. **28**(3), 257–271 (2005)

[2] Aarnes, J.E., Krogstad, S., Lie, K.A.: A hierarchical multiscale method for two-phase flow based upon mixed finite elements and nonuniform coarse grids. Multiscale Model. Simul. **5**(2), 337–363 (electronic) (2006)

[3] Aarnes, J.E., Krogstad, S., Lie, K.A.: Multiscale mixed/mimetic methods on corner-point grids. Comput. Geosci. **12**(3), 297–315 (2008). DOI 10.1007/s10596-007-9072-8. URL `http://dx.doi.org/10.1007/s10596-007-9072-8`

[4] Aavatsmark, I.: An introduction to multipoint flux approximations for quadrilateral grids. Comput. Geosci. **6**, 405–432 (2002). DOI 10.1023/A:1021291114475

[5] Aavatsmark, I., Barkve, T., Bøe, Ø., Mannseth, T.: Discretization on non-orthogonal, curvilinear grids for multi-phase flow. Proc. of the 4th European Conf. on the Mathematics of Oil Recovery (1994)

[6] Aziz, K., Settari, A.: Petroleum Reservoir Simulation. Elsevier Applied Science Publishers, London and New York (1979)

[7] Brezzi, F., Fortin, M.: Mixed and Hybrid Finite Element Methods, *Springer Series in Computational Mathematics*, vol. 15. Springer-Verlag, New York (1991)

[8] Brezzi, F., Lipnikov, K., Simoncini, V.: A family of mimetic finite difference methods on polygonial and polyhedral meshes. Math. Models Methods Appl. Sci. **15**, 1533–1553 (2005). DOI 10.1142/S0218202505000832

[9] Chen, Z., Hou, T.: A mixed multiscale finite element method for elliptic problems with oscillating coefficients. Math. Comp. **72**, 541–576 (2003)

[10] Christie, M.A., Blunt, M.J.: Tenth SPE comparative solution project: A comparison of upscaling techniques. SPE Reservoir Eval. Eng. **4**, 308–317 (2001). Url: `http://www.spe.org/csp/`

[11] Deutsch, C.V., Journel, A.G.: GSLIB: Geostatistical software library and user's guide, 2nd edn. Oxford University Press, New York (1998)

[12] Durlofsky, L.J.: Upscaling and gridding of fine scale geological models for flow simulation (2005). Presented at 8th International Forum on Reservoir Simulation Iles Borromees, Stresa, Italy, June 20–24, 2005

[13] Edwards, M.G., Rogers, C.F.: A flux continuous scheme for the full tensor pressure equation. Proc. of the 4th European Conf. on the Mathematics of Oil Recovery (1994)

[14] Efendiev, Y., Hou, T.Y.: Multiscale Finite Element Methods, *Surveys and Tutorials in the Applied Mathematical Sciences*, vol. 4. Springer Verlag (2009)

[15] Farmer, C.L.: Upscaling: a review. Int. J. Numer. Meth. Fluids **40**(1–2), 63–78 (2002). DOI 10.1002/fld.267

[16] Hou, T., Wu, X.H.: A multiscale finite element method for elliptic problems in composite materials and porous media. J. Comput. Phys. **134**, 169–189 (1997)

[17] Jenny, P., Lee, S.H., Tchelepi, H.A.: Multi-scale finite-volume method for elliptic problems in subsurface flow simulation. J. Comput. Phys. **187**, 47–67 (2003)

[18] Karypis, G., Kumar, V.: A fast and high quality multilevel scheme for partitioning irregular graphs. In: International Conference on Parallel Processing, pp. 113–122 (1995)

[19] Kippe, V., Aarnes, J.E., Lie, K.A.: A comparison of multiscale methods for elliptic problems in porous media flow. Comput. Geosci. **12**(3), 377–398 (2008). DOI 10.1007/s10596-007-9074-6. URL `http://dx.doi.org/10.1007/s10596-007-9074-6`

[20] Klausen, R.A., Stephansen, A.F.: Mimetic MPFA. In: Proc. 11th European Conference on the Mathematics of Oil Recovery, 8-11 Sept., Bergen, Norway, A12. EAGE (2008)

[21] Krogstad, S., Hauge, V.L., Gulbransen, A.F.: Adjoint multiscale mixed finite elements. SPE J. DOI 10.2118/119112-PA. SPE-119112-PA (in press; posted 23 August 2010)

[22] Ligaarden, I.S.: Well Models for Mimetic Finite Difference Methods and Improved Representation of Wells in Multiscale Methods. Master Thesis, University of Oslo (2008)

[23] Lipnikov, K., Shashkov, M., Yotov, I.: Local flux mimetic finite difference methods. Numer. Math. **112**(1), 115–152 (2009). DOI 10.1007/s00211-008-0203-5

[24] Manzocchi, T., Carter, J.N., Skorstad, A., Fjellvoll, B., Stephen, K.D., Howell, J.A., Matthews, J.D., Walsh, J.J., Nepveu, M., Bos, C., Cole, J., Egberts, P., Flint, S., Hern, C., Holden, L., Hovland, H., Jackson, H., Kolbjørnsen, O., MacDonald, A., Nell, P.A.R., Onyeagoro, K., Strand, J., Syversveen, A.R., Tchistiakov, A., Yang, C., Yielding, G., , Zimmerman, R.W.: Sensitivity of the impact of geological uncertainty on production from faulted and unfaulted shallow-marine oil reservoirs: objectives and methods. Petrol. Geosci. **14**(1), 3–15 (2008)

[25] The MATLAB Reservoir Simulation Toolbox, version 2010a (2010). URL `http://www.sintef.no/MRST/`

[26] Muskat, M.: The flow of homogeneous fluid through porous media. McGraw Hill Book Co., Inc, New York (1937)

[27] Natvig, J.R., Lie, K.A.: Fast computation of multiphase flow in porous media by implicit discontinuous Galerkin schemes with optimal ordering of elements. J. Comput. Phys. **227**(24), 10,108–10,124 (2008). DOI 10.1016/j.jcp.2008.08.024. URL `http://dx.doi.org/10.1016/j.jcp.2008.08.024`

[28] Notay, Y.: An aggregation-based algebraic multigrid method. Electronic Transactions on Numerical Analysis **37**, 123–146 (2010)

[29] Peaceman, D.W.: Interpretation of well-block pressures in numerical reservoir simulation with nonsquare grid blocks and anisotropic permeability. SPE, Trans. AIME **275**, 10–22 (1983)

[30] Skaflestad, B., Krogstad, S.: Multiscale/mimetic pressure solvers with near-well grid adaption. In: Proceedings of ECMOR XI–11th European Conference on the Mathematics of Oil Recovery, A36. EAGE, Bergen, Norway (2008)

[31] Zhou, H., Tchelepi, H.: Operator-based multiscale method for compressible flow. SPE J. **13**(2), 267–273 (2008)